Automatic and Real-Time Identification of Breathing Pattern from Ultrasound Liver Images

Jiaze Wu[1], Yanling Chi[1], Cheng Li[2], Bien Soo Tan[3], London Lucien Ooi[4], Satheesh Ramamurthy[3], and Jimin Liu[1]

[1] Singapore Bioimaging Consortium, Agency for Science, Technology and Research, Singapore
{wu_jiaze,liujm}@sbic.a-star.edu.sg
[2] Department of Bioengineering, National University of Singapore, Singapore
[3] Department of Diagnostic Radiology, Singapore General Hospital, Singapore
[4] Department of Surgery, Singapore General Hospital, Singapore

Abstract. In respiratory motion modeling for the liver, the breathing pattern is usually obtained by using special tracking devices from skin or diaphragm, and subsequently applied as input to a 4D motion model for motion estimation. However, due to the intrinsic limits and economical costs of these tracking devices, the identification of the breathing pattern directly from intra-operative ultrasound images is a more attractive option. In this paper, a new method is proposed to automatically track the breathing pattern from 2D ultrasound image sequences of the liver. The proposed method firstly utilizes a Hessian matrix-based 2D line filter to identify the liver boundary, then uses an adaptive search strategy to in real-time match a template block centered inside the identified boundary, and consequently extract the translational motion of the boundary as the respiratory pattern. The experiments on four volunteers demonstrate that the respiratory pattern extracted by our method is highly consistent to those acquired by an EM tracking system with the correlation coefficient of at least 0.91.

Keywords: ultrasound images, breathing pattern tracking, Hessian matrix-based filtering, adaptive search strategy.

1 Introduction

Image-guided robot-assisted surgery and intervention are now used in more and more hospitals to overcome limitations of traditional open and minimally invasive procedures. The most successful and established surgical robot system is the Da Vinci® operating system by Intuitive Surgical Inc. The issues with the Da Vinci system, however, are high cost of system and consumables, long set-up time for use and the absence of built-in intelligence. Despite these issues, it plays an established role in complex surgeries because of the value-added benefits but its use in simple procedures is conversely limited. To address the use of robots for simple procedures, a new trend in the medical devices is to develop simple image-guided, dedicated, low cost and easy-to-use robotic systems for specific surgical and/or interventional procedures.

C.A. Linte et al. (Eds.): MIAR/AE-CAI 2013, LNCS 8090, pp. 27–34, 2013.

Enlightened by the success of the prostate robot [1], we are developing an ultrasound (US) guided robot to achieve quantitatively targeted liver tumor biopsy and ablation, which requires accurate registration of pre-operative 3D computational tomography (CT) or magnetic resonance (MR) liver models to 2D intra-operative ultrasound images. However, the registration is challenging due to the movement and deformation of the liver soft tissue mainly caused by the respiration.

In order to compensate the respiration-induced motion, a possible solution is to track the targets using a 3D US probe [2], but the 3D US has limited scanning range, and produces large image data which causes the problems of processing, storing and transferring. Another potential scheme is to utilize a 2D US probe to track the target's in-plane motion, and move the probe swiftly to derive the out-of-plane motion [3]. The limitation of this method is that only a very thin slice near the plane is scanned, and the vibration of the probe can also reduce the imaging quality.

Therefore, at present, more attention is focused on model-based approach for the motion compensation [4]. With this approach, a pre-operative 4D whole liver motion model [5-7] or target-specific motion model [8, 9] is first created. During the intra-operative stage, a set of external or internal landmarks are tracked as the surrogate of respiratory pattern to drive the models to predict the liver motion. The external landmarks, applied on the abdomen or chest, are usually tracked using special optical or electromagnetic (EM) devices [8, 9]. These devices, however, create certain restrictions for the surgical robots. For example, there should be no optical or magnetic obstructs along the path of optical or electromagnetic tracker. On the other hand, as internal landmarks, the implanted fiducials [6] has the issue of invasiveness, and the diaphragm [7] requires an extra imaging device to track it. To overcome these problems, and particularly, to further reduce the cost of our surgical robot, and make it simple and portable, we wish to automatically identify the respiratory pattern from intra-operative US liver images.

Since the liver motion is strongly related to the respiration [10] and the liver boundary has relatively high contrast in 2D US images. Visually, the translational motion of the liver boundary in a fixed US imaging plane is quite related to the respiration pattern. In previous work [12], we discussed a manual way to select the liver boundary and extract the respiration pattern from the boundary. In this paper, we mainly present an automatic method to identify the liver boundary and extract its translational motion as respiratory pattern.

2 Materials and Methods

2.1 Overview

The main framework of our method is shown in Fig. 1, which is roughly divided into three main stages: 1) acquisition of US image sequences; 2) automatic identification of the liver boundary; 3) fast extraction of the breathing pattern. The experiment settings for acquiring the US images are elaborated in subsection 2.2.

After acquired, the first image of the image sequence is selected as the reference image for the following identification. The liver boundary will be recognized by a

serial of consecutive processes (Fig. 1), namely filtering (enhancing the liver boundary and removing other parts in the reference image), masking (eliminating the periphery of the filtered image), thresholding (removing the weak non-boundary part), and finding the largest connected part (i.e. the liver boundary). Subsection 2.3 will describe the Hessian-based 2D line filter, which plays a key role in recognizing the liver boundary.

After the liver boundary is recognized, a template block (65×65 pixels by experiments), whose center is located inside the liver boundary, is automatically selected from the reference image of the image sequence. Using this template block, a frame-by-frame matching process, based on the normalized correlation (NC) similarity metric and adaptive search range, is executed to extract the breathing pattern. The search range on the current frame is adaptive because its center is updated as the optimally matched position of the former frame. Subsection 2.4 gives a detailed explanation on this search strategy, which makes use of the inter-frame dependency.

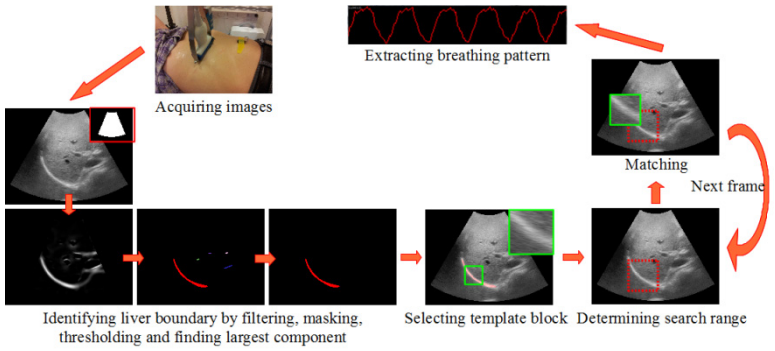

Fig. 1. The processing flow of our method for identifying and extracting the breathing pattern. It consists of three basic consecutive stages: 1) acquisition of image sequences; 2) identification of the liver boundary; 3) extraction of the breathing pattern.

2.2 Data Acquisition

The US image sequences (image resolution of 640 × 480 pixels, pixel size of about 0.37 × 0.37 mm and temporal resolution of 10 FPS) for analysis are acquired from four healthy volunteers (male, average age 36, ranged 25-46), and each sequence consists of 256 frames. The used US imaging system is the Terason t3000 with a 5C2 transducer. In order to validate the breath pattern identified by our method, a NDI Aurora electromagnetic (EM) tracking system is used to track an EM sensor on the umbilicus of the volunteers while acquiring the US images. The motion of umbilicus is selected as the reference breathing pattern for evaluation because the umbilicus on the abdominal surface is usually a good position to monitor the abdominal respiration [4]. By using the dynamic libraries from NDI and Terason, we implemented a module in our software platform to synchronously record the US images and EM signals, each US frame corresponding to an EM position. Actually, each EM position has 3

components (x, y, z), but we only need to choose one of them, which changes highly correspond to the movement of the skin marker. In order to avoid the tremor of the US probe by hands, a robotic arm is designed to fix the probe, which can stably acquire the images.

2.3 Hessian-Based 2D Line Filter

We introduce a 2D line filter to selectively enhance the line-like structures (mainly the liver boundary) in US liver images and filter out other non-line structures. This filter is inspired by Frangi's multi-scale line filter [11], which was designed to enhance the vessels of different sizes in 2D digital subtraction angiography (DSA) and 3D magnetic resonance angiography (MRA) images. In this paper, the liver boundary, which we are interested in, may be regarded as a vessel-like structure of strong contrast, which is observed in the US images of Fig. 1. However, compared to the multi-scale nature of Frangi's filter simultaneously considering the vessels of various sizes in images, our filter is of single scale only dependent on the width of the liver boundary.

Our line filter is on the basis of the eigenvalues of the Hessian matrix, which represents the second-order local structures of an image. The filtering process can be roughly divided into three basic consecutive steps:

1) **Gaussian-based smoothing.** A Gaussian filter $G(\boldsymbol{x};\sigma)$ with standard deviation σ is employed to smooth the each pixel $I(\boldsymbol{x})$ of the 2D image I, where $\boldsymbol{x} = (x, y)$ denotes a pixel location in the image;

2) **Calculation of Hessian matrix and its eigenvalues.** The Hessian matrix $H(\boldsymbol{x};\sigma)$ of each pixel $I(\boldsymbol{x})$ of the filtered image $I(\boldsymbol{x};\sigma)$ is calculated by

$$H(\boldsymbol{x};\sigma)=\nabla I(\boldsymbol{x};\sigma)=\begin{bmatrix} I_{xx}(\boldsymbol{x};\sigma) & I_{xy}(\boldsymbol{x};\sigma) \\ I_{yx}(\boldsymbol{x};\sigma) & I_{yy}(\boldsymbol{x};\sigma) \end{bmatrix}, \tag{1}$$

where partial second-order derivatives of the filtered image $I(\boldsymbol{x};\sigma)$ at the pixel location $\boldsymbol{x}$ are denoted by $I_{xx}(\boldsymbol{x};\sigma)$, $I_{xy}(\boldsymbol{x};\sigma)$ and so on. Assume that $\lambda_1(\boldsymbol{x};\sigma)$ and $\lambda_2(\boldsymbol{x};\sigma)$ are the eigenvalues of the Hessian matrix $H(\boldsymbol{x};\sigma)$, and satisfy $|\lambda_1(\boldsymbol{x};\sigma)| \le |\lambda_2(\boldsymbol{x};\sigma)|$;

3) **Resulting filtering.** By combination of both eigenvalues, the resulting response is calculated by [11]

$$V(\boldsymbol{x};\sigma)=\begin{cases} 0 & \text{if } \lambda_2(\boldsymbol{x};\sigma)>0 \\ \exp\left(-\dfrac{R^2(\boldsymbol{x};\sigma)}{2\beta^2}\right)\left(1-\exp\left(-\dfrac{S^2(\boldsymbol{x};\sigma)}{2c^2}\right)\right) & \text{otherwise,} \end{cases} \tag{2}$$

where $R(\boldsymbol{x};\sigma)=\lambda_1(\boldsymbol{x};\sigma)/\lambda_2(\boldsymbol{x};\sigma)$ measures the blobness of each pixel in the image, $S(\boldsymbol{x};\sigma)=\sqrt{\lambda_1^2(\boldsymbol{x};\sigma)+\lambda_2^2(\boldsymbol{x};\sigma)}$ defines the local second-order structureness of each

pixel, and β and c decide the sensitivity of the line filter to both measures $R(\boldsymbol{x};\sigma)$ and $S(\boldsymbol{x};\sigma)$.

The blobness measure will gain small values in the blob-like structures or background, but large values in the line-like structures, for instance the liver boundary. On the other hand, the structureness measure will be fairly low in the background where no outstanding objects are present, but in regions with high contrast, the measure will be comparatively high. Therefore, both measures are glued together to achieve the selective response of this filter on the line structures, and ignore the blob structures or background. In all the experiments of this paper, β is fixed to 0.5. The value of c depends on the grey-scale range of the image and half the value of the maximum Hessian norm has proven to work in most cases [11].

2.4 Adaptive Search Strategy

Due to the quasi-periodicity of the normal respiration, the liver tissue also moves in an approximately periodical way. Therefore, the liver tissue repeatedly appears in a relatively fixed extent (the maximal motion appears in the superior-inferior direction with the range of 5-25 mm [10]) in a normal or even deep breathing cycle, and the search range can be restricted as a medium extent. Our experiment shows that a region of 129×129 pixels is required to find the optimal match. During the frame-by-frame matching process, the traditional search strategy is to fix the center of the search range according to the position of the template region on the reference image, which is called as *center-fixed search strategy*, which is time-consuming and cannot satisfy the real-time requirement for the motion tracking.

Motivated by this problem, we present a new *adaptive search strategy* [12], which defines a serial of small center-variant search ranges along the frame-by-frame matching process. Our search strategy makes full use of the inter-frame dependency of the US image sequence, which assumes that the motion extent of the liver tissue is small for two successive frames. Therefore, any specified image block on the former frame should appear inside the small neighbor region of the same position on current frame. The optimal matching position of the former frame can be used as the center of the search range of the current frame. Based on this principle, a serial of relatively small search ranges (17×17 pixels), whose centers are automatically updated according to the former matched result, are formed along the image sequence. Here, we call center-variant search range as *adaptive search range*. Using the adaptive search strategy, we may quickly extract the respiratory pattern from the liver boundary.

3 Results

Fig. 2 shows the gradually varying filtering responses by tuning the smooth scale parameter in Eq. (2). The results show that this filter gains strongest response near the scale $\sigma = 11$ where the filtered boundary is maximally close to that in the original image. The experiments on various US images from four volunteers also support this

conclusion. Therefore, in all the following experiments of this paper, the smooth scale is fixed to 11. These experiments also prove the scale parameter is roughly proportional to the width of the liver boundary.

Fig. 3 shows the selectivity characteristic of the Hessian matrix-based line filter, where four sample images scanned from four corresponding volunteers are filtered. It is observed that the response has high value at the liver boundary and other line structures of high contrast. Since the smooth scale is set to fit the liver boundary and the boundary has higher contrast than other line-like structures, the response is strongest near the boundary. Therefore, as expected, the liver boundary can always be selectively preserved by the subsequent thresholding and largest-region-selection.

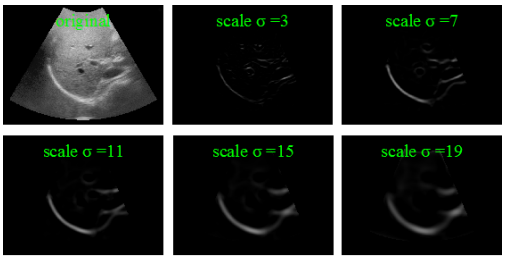

Fig. 2. Responses of our line filter under different smoothing scales. The strongest response on the liver boundary is gained at the scale $\sigma = 11$, which simultaneously most approximates the boundary in the original image.

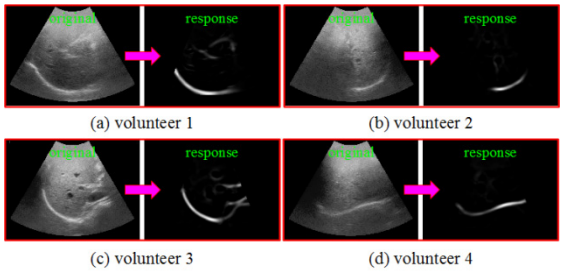

Fig. 3. The sample images (left one of each image pair) from four volunteers are processed by the line filter, and the response is strongest near the liver boundary

In order to validate our method, we chose the movement of the umbilicus on the abdominal skin as the reference breathing pattern. Four image sequences from three corresponding volunteers were used for processing, and, for each image sequence, two exemplary image blocks centered inside the recognized liver boundary were selected as matching templates. The extracted breathing patterns (Fig. 4, plotted in red) were visually compared to the reference breathing patterns of the umbilicus (Fig. 4, in green). A visual inspection on both patterns shows that the extracted breathing patterns are highly consistent with the reference ones. For convenience of visual inspection, all motion curves, including the reference ones, were normalized to the interval

of 0 to 1. Using the correlation coefficient (CC) metric, the extracted breathing patterns by our method were quantitatively compared to the reference ones. The results from Table 1 show high relevance between both kinds of breathing patterns, which can be explained by that the motions of the liver and the abdominal skin are all induced by the respiration.

In addition, we also performed a quantitative analysis on the computation efficiency of our method, which is listed in Table 2. It is noticed that our adaptive search method can extract the breathing patterns in about 5 seconds for an image sequence of 256 frames, whereas the traditional search method takes nearly 6 minutes. These experiments were executed on a Dell workstation with Intel Xeon CPU E5620 2.4 GHz and 12G RAM, and the single-thread programming mode was used.

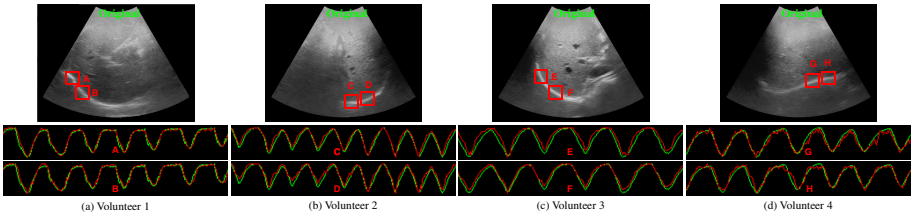

Fig. 4. Consistency is visually compared between the breathing patterns (in red), identified by our method, and the EM-tracked reference patterns of the umbilicus (in green). 8 template blocks from 4 volunteers' image sequences of 256 frames are used.

Table 1. The consistency between the extracted breathing patterns and the reference breathing patterns is analyzed using the correlation coefficient (CC). The image sequences are the same as Fig. 4.

	Volunteer 1		*Volunteer 2*		*Volunteer 3*		*Volunteer 4*	
Blocks	A	B	C	D	E	F	G	H
Relevance	0.9559	0.9541	0.9511	0.9379	0.9844	0.9784	0.9172	0.9206

Table 2. The computation time between the traditional search strategy and our adaptive strategy is compared. The image sequences are the same as Fig. 4, and the time unit is second.

		Volunteer 1		*Volunteer 2*		*Volunteer 3*		*Volunteer 4*	
Blocks		A	B	C	D	E	F	G	H
Time (s)	Traditional	301.4	299.6	260.0	278.0	299.4	299.7	290.8	291.7
	Adaptive	5.19	5.22	5.17	5.19	5.22	5.14	5.07	5.05

4 Conclusion

We have introduced an efficient Hessian matrix-based 2D line filter to automatically identify the liver boundary from the ultrasound image sequences, and then proposed an adaptive block matching method to extract the translation motion of the liver boundary as the respiratory pattern. The experiments have also demonstrated that our

method can automatically and precisely recognize the liver boundary, and in several seconds extract the breathing pattern, which is in phase comparable to that of the EM tracking system. This will be of great help for US-guided surgical robots to have a build-in respiratory signal tracking system, resulting in a more compact and flexible design at low cost.

References

1. Ho, H., Yuen, J.S.P., Cheng, C.W.S.: Robotic prostate biopsy and its relevance to focal therapy of prostate cancer. Nature Reviews Urology 8, 579–585 (2011)
2. Bruder, R., Ernst, F., Schlaefer, A., Schweikard, A.: A Framework for Real-Time Target Tracking in Radiosurgery using Three-dimensional Ultrasound. In: CARS 2011, pp. S306–S307 (2011)
3. Nadeau, C., Krupa, A., Gangloff, J.: Automatic Tracking of an Organ Section with an Ultrasound Probe: Compensation of Respiratory Motion. In: Fichtinger, G., Martel, A., Peters, T. (eds.) MICCAI 2011, Part I. LNCS, vol. 6891, pp. 57–64. Springer, Heidelberg (2011)
4. McClelland, J.R., Hawkes, D.J., Schaeffter, T., King, A.P.: Respiratory motion models: A review. Medical Image Analysis 17, 19–42 (2012)
5. Rohlfing, T., Maurer, C.R., O'Dell, W.G., Zhong, J.: Modeling liver motion and deformation during the respiratory cycle using intensity-based nonrigid registration of gated MR images. Medical Physics 31, 427–432 (2004)
6. Preiswerk, F., Arnold, P., Fasel, B., Cattin, P.C.: Robust tumour tracking from 2D imaging using a population-based statistical motion model. In: IEEE Workshop on Mathematical Methods in Biomedical Image Analysis, pp. 209–214 (2012)
7. Rijkhorst, E.-J., Rivens, I., ter Haar, G., Hawkes, D., Barratt, D.: Effects of Respiratory Liver Motion on Heating for Gated and Model-Based Motion-Compensated High-Intensity Focused Ultrasound Ablation. In: Fichtinger, G., Martel, A., Peters, T. (eds.) MICCAI 2011, Part I. LNCS, vol. 6891, pp. 605–612. Springer, Heidelberg (2011)
8. Khamene, A., et al.: Characterization of Internal Organ Motion Using Skin Marker Positions. In: Barillot, C., Haynor, D.R., Hellier, P. (eds.) MICCAI 2004. LNCS, vol. 3217, pp. 526–533. Springer, Heidelberg (2004)
9. Ernst, F., Martens, V., Schlichting, S., Beširević, A., Kleemann, M., Koch, C., Petersen, D., Schweikard, A.: Correlating Chest Surface Motion to Motion of the Liver Using ε-SVR – A Porcine Study. In: Yang, G.-Z., Hawkes, D., Rueckert, D., Noble, A., Taylor, C. (eds.) MICCAI 2009, Part II. LNCS, vol. 5762, pp. 356–364. Springer, Heidelberg (2009)
10. von Siebenthal, M.: Analysis and modelling of respiratory liver motion using 4DMRI. Ph.D. thesis, ETH Zurich (2008)
11. Frangi, A.F., Niessen, W.J., Vincken, K.L., Viergever, M.A.: Multiscale vessel enhancement filtering. In: Wells, W.M., Colchester, A.C.F., Delp, S.L. (eds.) MICCAI 1998. LNCS, vol. 1496, pp. 130–137. Springer, Heidelberg (1998)
12. Wu, J., Li, C., Huang, S., Liu, F., Tan, B.S., Ooi, L.L., Yu, H., Liu, J.: Fast and robust extraction of surrogate respiratory signal from intra-operative liver ultrasound images. International Journal of Computer Assisted Radiology and Surgery (publish online, 2013)